



SIST '18

## A CONCEPT FOR ULTRA-HIGH ENERGY ELECTRON AND POSITRON TEST BEAMS AT FERMILAB

Jamal Johnson

Pittsburg State University

Carol Johnstone, Ph. D (Supervisor)

Fermilab, Accelerator Division

### Abstract

This project is a feasibility study in the production of a high energy ( $>30$  GeV) electron ( $e^-$ ) and positron ( $e^+$ ) beam created from secondary particles of a 120 GeV/c proton beam incident upon a target. The primary source of high energy  $e^\pm$  was believed to be a rare decay channel of charged pions. Under this assumption an ideal material was selected and its dimensions optimized for prompt charged pions. The unexpected presence of high energy prompt  $e^\pm$  also led to additional optimization for maximizing their production. The bulk intensity to expected at the experiment (with assumed losses from future separation optics) was studied via magnetic transport simulation. Ultimately, both minimum requested intensity and energy were greatly exceeded via use of a Beryllium target sited in current test beamlines and enclosures. This was done with target dimensions optimized for  $\pi^-$  production as more time was needed to compare the results from the other species-specific dimensional optimizations. Additional optimization would potentially yield greater secondary particle intensities.

## 1. Introduction

This project is a feasibility study in the production of a high energy (>30 GeV) electron ( $e^-$ ) and positron ( $e^+$ ) beam produced as secondary particles from a beam of 120 GeV/c protons incident upon a target. The primary source of high energy  $e^\pm$  was believed to be a rare decay channel of charged pions. Under this assumption, a target material was selected and its dimensions optimized for charged pion production. The beam dynamics program, G4Beamline, was used to simulate the interaction of the proton beam with a Beryllium target selected during target-material optimization. In this work, it was found that high energy prompt  $e^\pm$  production greatly exceeded  $e^\pm$  from decay of pions. Electron and positron yields are compared here for both production mechanisms.

In order to calculate the intensity of high energy  $e^\pm$  beams that can be delivered to an experimental site, transmission as a function of distance was studied in a magnetic transport channel. An alternating-gradient strong-focusing (FODO) channel was designed to transport the electron and positron beams, specifically for particles with a momentum of 50 GeV/c and a momentum range about this central value (referred to here as a momentum bite) of 5%. This FODO channel was implemented in G4Beamline, and both prompt  $e^\pm$  and charged pions were propagated up to ~500 m from the center of the target. The results from this study showed that  $e^\pm$  at 50 GeV/c and this momentum spread achieved a production rate per proton-on-target (POT) of  $5 \times 10^{-6}$  for  $e^-$  and  $4 \times 10^{-6}$  for  $e^+$ . At the current proton test-beam intensity of  $2 \times 10^{11}$ , this yields  $5 \times 10^5$   $e^-$  and  $4 \times 10^5$   $e^+$  within the given momentum bite and upstream solid angle of the transport beamline. Even estimating losses in intensity of an order of magnitude after beam capture and transport with magnetic optics, the electron and positron population still exceeds the minimum specifications from users of the Fermilab Test Beam Facility (FTBF) beam – 5,000  $e^-$  or  $e^+$  per 4 second spill – by a factor of 10. At the maximum intensity,  $1 \times 10^{13}$  protons over the 4 sec slow spill, which is supported by another Fermilab external beamline, this specification is exceeded by a factor of 1000.

Though the results of the study were successful in producing an electron and positron test beam, simulation data were collected from a target whose dimensions were optimized for charged pion production. Additional studies are needed to optimize  $e^\pm$  production for the highest intensity and energy achievable for electron and positron test beams at Fermilab.

## 2. Background

With the planned 2-year shutdown of CERN test beams, test-beam users requiring  $e^\pm$  beams with an energy higher than 30 GeV will require a new facility for their research.<sup>1,10</sup> The energy (which for low mass particles such as  $e^\pm$  is very close to its momentum magnitude) of CERN test beams currently exceeds comparable  $e^\pm$  beams at DESY (whose beams are under 10 GeV/c) and SLAC (whose  $e^-$  beam is limited to 25 GeV/c). The limitations of available  $e^\pm$  beams during CERN's shutdown will provide Fermilab a unique opportunity to attract a new group of users, if a higher energy test beam of at least 5,000 particles per spill can be designed and implemented.<sup>2,3</sup> In addition to the energy and intensity needs of users, offering a pure beam, not mixed with other species (the CERN test beams are mixed-particle species beams) would satisfy the 3 major attributes electron and positron beam users are requesting. Key applications of the higher energy, pure  $e^\pm$  in conducting in-house calibration of particle detector calorimeters is also desired.

Optimization of a target for secondary  $e^\pm$  production using the Fermilab Main Injector 120 GeV proton beam comprised the major objective of this study. It was initially believed that the following

rare charged pion decay (with a branch fraction of 0.000123) would yield the highest energy  $e^\pm$  beams.<sup>4</sup>



Thus, maximizing the production of prompt charged pions was pursued and used as the initial design criterion in selection of target material and dimensions.

Preliminary calculations were conducted to quantify the expected yield of  $e^\pm$  at the experiment site and the  $\pi^\pm$  production needed to meet the minimum requested intensity of  $e^\pm$  for various energies above 30 GeV.

Using a momentum of 50 GeV/c, the expected  $\pi^\pm$  decay and fraction expected to branch to  $e^\pm$  upon reaching the experiment were calculated for obtaining ~50 GeV  $e^\pm$ .

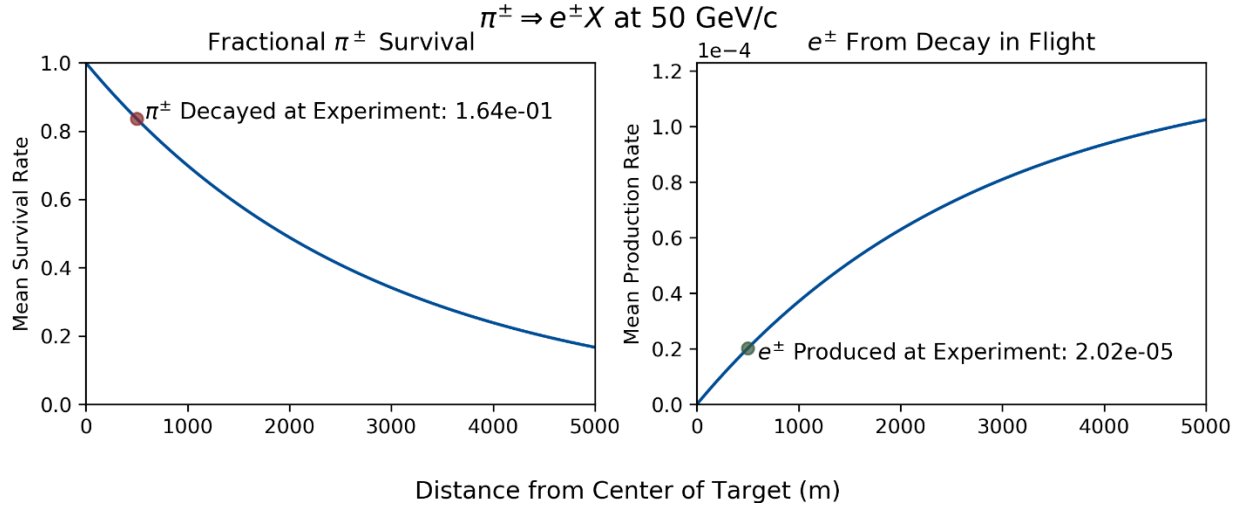


Figure 1 | Fractional Decay in Flight for 50 GeV/c  $\pi^\pm$  and Prompt  $e^\pm$ . At the experiment distance of 500 m only a small portion of  $\pi^\pm$  will have decayed, and even less into  $e^\pm$ . For higher momentum (or higher velocity)  $\pi^\pm$ , even less decay will have occurred as it reaches the experiment faster.

The minimal  $\pi^\pm$  per proton-on-target (POT) needed to achieve 5,000 secondary electrons or positrons for various momentum bites at the experimental site was computed for comparison with operational primary intensities. The average rest mass ( $m_0$ ) 139.57018 MeV/c<sup>2</sup> and average mean lifetime ( $\tau_{ml}$ )  $2.60 \times 10^{-8}$  s for  $\pi^\pm$  were used, as well as the speed of light  $c$ . Computing the relativistic factor  $\gamma$ , the velocity ( $v$ ), and particle flight time to the experiment ( $t_f$ ) was done using the following formulas.

$$\gamma = \left(1 + \left(\frac{P}{m_0 c}\right)^2\right)^{1/2} \quad (3)$$

$$v = \frac{P}{\gamma m_0} \quad (4)$$

$$t_f = \frac{500 \text{ meters}}{v} \quad (5)$$

The values obtained were then used to find the fraction decayed ( $N_d$ ) of  $\pi^\pm$  expected at the experiment.

$$N_d(t_f, \gamma) = 1 - \exp\left(-\frac{t_f}{\gamma\tau_{ml}}\right) \quad (6)$$

Using the current proton beam intensity  $2 \times 10^{11}$  as the POT value and the branch fraction for (1) & (2), the minimum prompt (denotes particles produced directly from a target)  $\pi^\pm$  per POT needed to produce  $5 \times 10^4$   $e^\pm$  at the experiment was computed via

$$\text{Minimum } \frac{\pi^\pm}{\text{POT}} = \frac{5e4}{1.23e^{-4} \times \text{POT} \times N_d} \quad (7)$$

To examine the how the minimum needed production rate for a  $\pm 5\%$  momentum bite varies, a central momentum of 50 GeV/c was studied in Table 1.

Prompt $\pi^\pm$ :					
Minimum Production for $5E04$ $e^\pm$ at Experiment for 50 GeV/c $\pm 5\%$ p Bite					
Momentum (GeV/c)	Relativistic Factor $\gamma$	Velocity (fraction of c)	Flight Time to 500 m (s)	Pion Decay (fraction of 1)	Minimum Production Needed with $2e11$ POT ( $\pi^\pm/\text{proton}$ )
47.5	340.3320469	0.999995683	1.667827676E-06	0.171588516	1.1845E-02
50	358.2441091	0.999996104	1.667826974E-06	0.163754478	1.2412E-02
52.5	376.1561784	0.999996466	1.667826370E-06	0.156602722	1.2979E-02

Table 1 | Minimum Prompt  $\pi^\pm$  per POT Production Required for  $5 \times 10^4$   $e^\pm$  at Experiment Within the 50 GeV/c  $\pm 5\%$  Momentum Bite. Relative to the production rate required for 50 GeV/c, the differences on the lower and upper ends of the momentum bite were calculated to be about  $\pm 0.0006$   $\pi^\pm / \text{POT}$ . As this small difference was seen to be negligible, only production rates at the central values of several momenta were calculated for comparison next.

With minimal differences in production over a given momentum bite understood, central momentum values corresponding to higher energy  $e^\pm$  were used to calculate production of  $\pi^\pm$  needed to satisfy desired intensity at the experiment in Table 2.

Prompt $\pi^\pm$ :					
Minimum Production For $5E04$ $e^\pm$ at Experiment for 40, 50, 60, 70, and 80 GeV/c					
Momentum (GeV/c)	Relativistic Factor $\gamma$	Velocity (fraction of c)	Flight Time to 500 m (s)	Pion Decay (fraction of 1)	Minimum Production Needed with $2e11$ POT ( $\pi^\pm/\text{proton}$ )
40	286.5959154	0.999993913	1.667830629E-06	0.200318118	1.0146E-02
50	358.2441091	0.999996104	1.667826974E-06	0.163754478	1.2412E-02
60	429.8924192	0.999997294	1.667824988E-06	0.138454594	1.4680E-02
70	501.5407958	0.999998012	1.667823791E-06	0.119915958	1.6950E-02
80	573.1892138	0.999998478	1.667823014E-06	0.10575066	1.9220E-02

Table 2 | Minimum Prompt  $\pi^\pm$  per POT Production Required for  $5 \times 10^4$   $e^\pm$  at Experiment at 40, 50, 60, 70, and 80 GeV/c. Obtaining sufficient intensities of higher momentum  $e^\pm$  requires higher production of  $\pi^\pm$  from target.

## 2.1 Nuclear Interaction Length vs Radiation Length and Pion Interaction Length

The nuclear interaction length of a material describes the interaction of heavy particles (such as protons) with nuclei.<sup>5</sup> Since charged pions are produced from nuclear interactions (primarily high energy collisions between hadrons), a material with a short nuclear interaction length was selected to maximize the probability of these interactions with target length.

The radiation length gives the average distance in a material at which electrons lose 1/e of their energy.<sup>5</sup> However, radiation length also describes the effect of multiple small angle deflections caused by the Coulomb interaction – see equation below. It is important to optimize the electron or positron beam properties by minimizing its transverse dimensions and divergence in order to capture and transport the secondary beam – thus one wants a large radiation length to minimize multiple Coulomb scattering; i.e the ratio of the nuclear interaction length / radiation length should be minimized for optimal target choice (more on this in 2.3). This measurement of beam properties, transverse size x divergence, accounts for both the angular spread and transverse space occupied by beam exiting the target. It is referred to as the emittance (the root mean squared emittance is denoted via  $\theta_{rms}$ ).<sup>6</sup> To achieve minimal emittance, the longest radiation lengths and shortest interaction lengths guided the choice of beryllium as the target material.

$$\theta_{rms} = \frac{13.6 \text{ MeV}}{\beta c p} \sqrt{x/X_0 \left[ 1 + 0.038 \ln \left( x/X_0 \right) \right]} \quad (8)$$

In the equation above,  $\beta c$  is velocity (where  $\beta$  is a unitless value obtained from the ratio of the particle's speed to the speed light  $c$ ),  $p$  is momentum in GeV/c,  $x$  the length of the target, and  $X_0$  the radiation length of the target.

Additionally, the pion interaction length gives an average distance within a material that pions will traverse before an inelastic interaction occurs and the pion potentially does not escape the target material. Though not fully understood, it was believed that these interactions may lead to a greater degree of pion scattering or collisions strong enough to break the pion into its constituent quarks (leading to the formation of other particles). To decrease the probability that this would occur, a longer pion interaction length was needed to extract as many pions as possible from the target.

## 2.2 G4Beamline and the Monte Carlo Method

G4Beamline is a program that tracks charged particles through magnetic and electric fields and is optimized for beamline design.<sup>7</sup> It is based on GEANT4, an object-oriented program developed at CERN in 1998, that simulates the passage and interactions of particles with matter. The output of GEANT4 is a data text file providing all kinematical variables for each particle received at a user defined detector, such as x, y, z positions in mm, the respective components of momentum,  $p_x$   $p_y$   $p_z$  in MeV/c, particle ID#, and more. All physics processes used in G4Beamline come from GEANT4 and can be found in the comprehensive physics lists, which must be individually selected when running a simulation.<sup>8</sup>

Known as single particle tracking, G4Beamline simulates one primary particle at a time and tracks its interaction with matter. Probabilities regarding the production of secondary particles from the primary (via the various processes handled by the physics list) are governed by the Monte Carlo Method<sup>7,8</sup>. This is a statistical method that uses randomly generated inputs for specified physics processes to cover the spectrum of possible outcomes. The results produced are expressed as the mean of the normal, or Gaussian, distribution describing the statistical distribution of primary or secondary beams after interacting. One unit of standard deviation ( $\sigma$ ) of the distribution for the value returned (for N particles) is the root of N. The simulation or prediction thus becomes increasingly accurate the higher the number of particles tracked (or the higher the

primary intensity) since the error or standard deviation is  $\sqrt{N}$ , making it ideal for high intensity particle beam simulations <sup>9</sup>.

### 2.3 Quadrupole Magnets and Alternating Gradient Focusing

In order to propagate the beam to the experiment site, quadrupole magnets (or quads for short) are used to focus beam in the transverse (x, y Cartesian coordinate system with z the direction of the beam) plane.

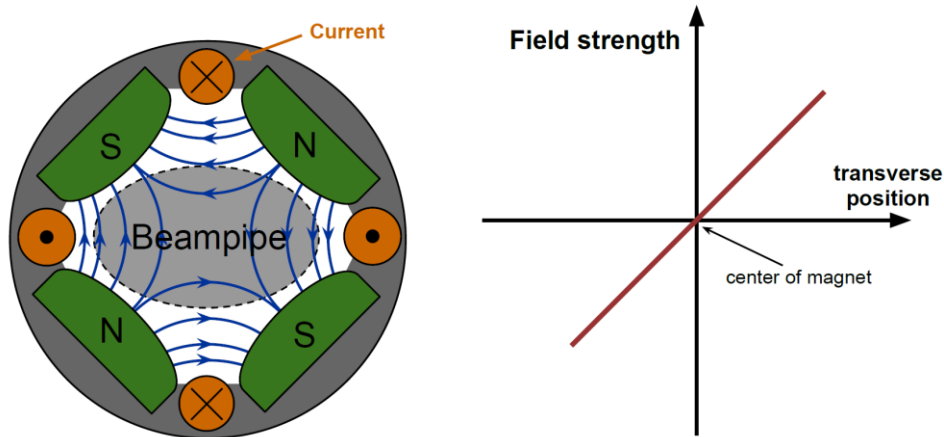


Figure 2 | Quadrupole magnetic field direction and current direction (left) and field strength in relation to transverse displacement from the center (right).<sup>6</sup> Along the longitudinal axis of the quad (the z-axis is assumed centered at the magnet's aperture), the magnetic field strength is zero. However, a transverse displacement from the center experiences a linear increase of the field's strength with distance, and the field focuses or defocuses off-axis particles. These factors change the angle of a particle and the overall divergence or convergence of the beam envelope.<sup>6</sup>

Though quads serve to focus the beam, individual quads are not able to achieve simultaneous focusing in the vertical and horizontal transverse dimensions.

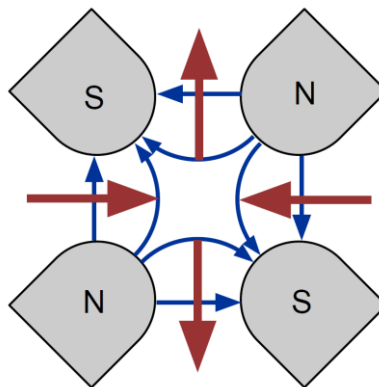


Figure 3 | Quadrupole Magnet Field and Effective Force Direction on Charged Particles with Longitudinal Velocity.<sup>6</sup> The magnetic field direction (blue lines) and the direction of force (the focusing direction) experienced by charged particles within the beam (red arrows) is shown.<sup>6</sup>

Quads that focus in the horizontal plane while defocusing in the vertical plane are referred to as focusing magnets (denoted with an F), while quads that focus in the vertical plane while

defocusing in the horizontal plane are called defocusing magnets (denoted by D). The drift space between successive quads is designated with an O. What controls whether a quad will be a focusing magnet or defocusing magnet is its polarity, which in turn is controlled by the directions of current through the magnet (reference Figure 1). Changing the polarity reverses the direction of the field's gradient within the magnet. By convention, F quads have a positive gradient, while D quads have a negative gradient.

Analogous to the focusing and defocusing of light by lenses, quads also have a focal length. However, an important difference is that it is not constant but dependent on the momentum of the particle. Higher momentum particles will be bent less by the magnetic field with a focal point further downstream from the quad than lower momentum particles.

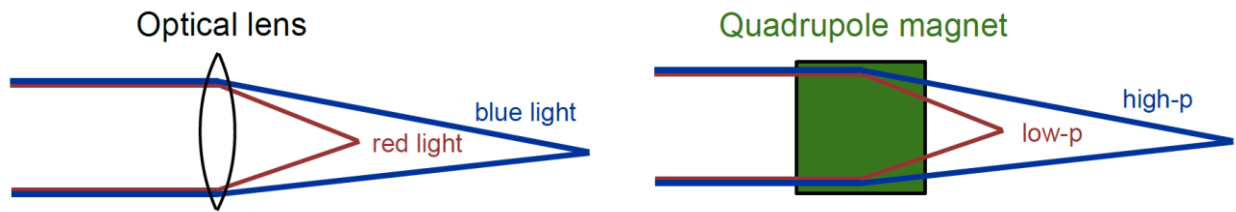


Figure 4 | Lens and Quadrupole Magnet Optical Focusing Comparison.<sup>6</sup> Similar to the focusing of higher frequency light focused through a lens (left), higher momenta charged particles achieve maximal focusing further from the magnet than charged particles of lower momenta (right).<sup>6</sup>

To achieve overall beam confinement simultaneously in horizontal and vertical planes, F and D quads are alternated to form a lattice. This is a technique known as alternating gradient focusing or strong focusing.

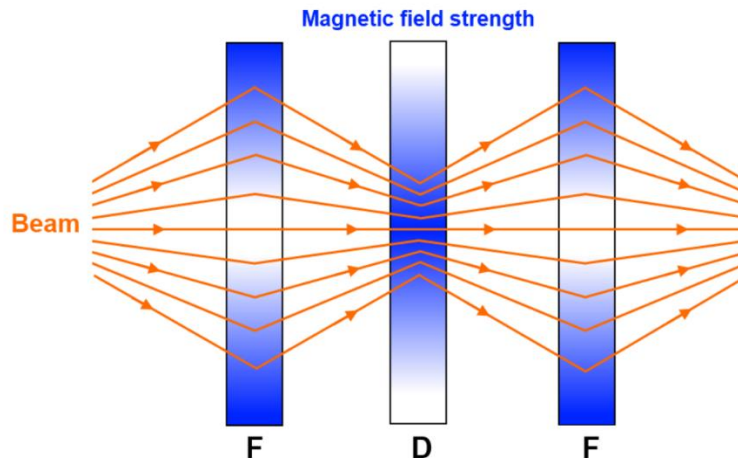


Figure 5 | Alternating Gradient Focusing.<sup>6</sup> The blue-white color gradient represents the magnetic field gradient in focusing and defocusing quadrupoles.<sup>6</sup>

The repetitive unit of the lattice is a single F and D quad, known as a FODO cell or cell here for short. The drift distance between the quads (denoted with an O) is important as it must be less than the distance of the focal length as given by the quad strength.<sup>6</sup>

### 3. Methodology

#### 3.1 Secondary Particle Production and Preliminary Design

To better understand the angular and energy spread of the high energy secondary particles, some initial simulations in G4Beamline were performed. Secondary particle production was simulated using a 120 GeV primary proton beam incident on a beryllium target with a Gaussian distribution. The distribution has a standard deviation ( $\sigma$ ) in transverse position of 5 mm in both the x ( $\sigma_x$ ) and y ( $\sigma_y$ ) dimensions and an initial primary intensity of  $1 \times 10^4$  protons (though this was later increased to  $1 \times 10^6$  protons as referenced in Figure 7). Secondary particles were recorded using a flat disk detector at a radius 1 m from the target center. Observations of the emittance of higher energy (>30 GeV) particles were recorded with this software detector. The raw particle data was then parsed and studied with Python 3.6.4 using NumPy, SciPy, Matplotlib, and Math libraries. The majority of analysis code was created in Jupyter Notebook™.

To understand the data, the coordinate system convention is defined as follows (reference Figure 5). The positive z-axis is defined as the initial forward direction of the incident proton beam, the upward transverse direction is positive y, the azimuthal plane, beam left, is positive x with the origin placed at the center of the target. The angle within the xz-plane with zero radians being any point on the positive z-axis was defined as the bearing. Similarly, the angle in the yz-plane with any point on the positive z-axis being zero radians, was defined as the pitch.

Anticipating that the beam would require collimation since a large solid angle cannot be transported by the focusing magnets, the detector was dimensioned to receive particle data for those with pitch narrow enough to enter a 2 inch vertical aperture. This aperture is realistically matched to that of the magnetic component apertures. Since a collimator could be placed 1 m from the center of the target, the cylindrical detector was given a 1 m radius and positioned so that its origin overlapped the center of the target.



## G4Beamline Visualization Mode

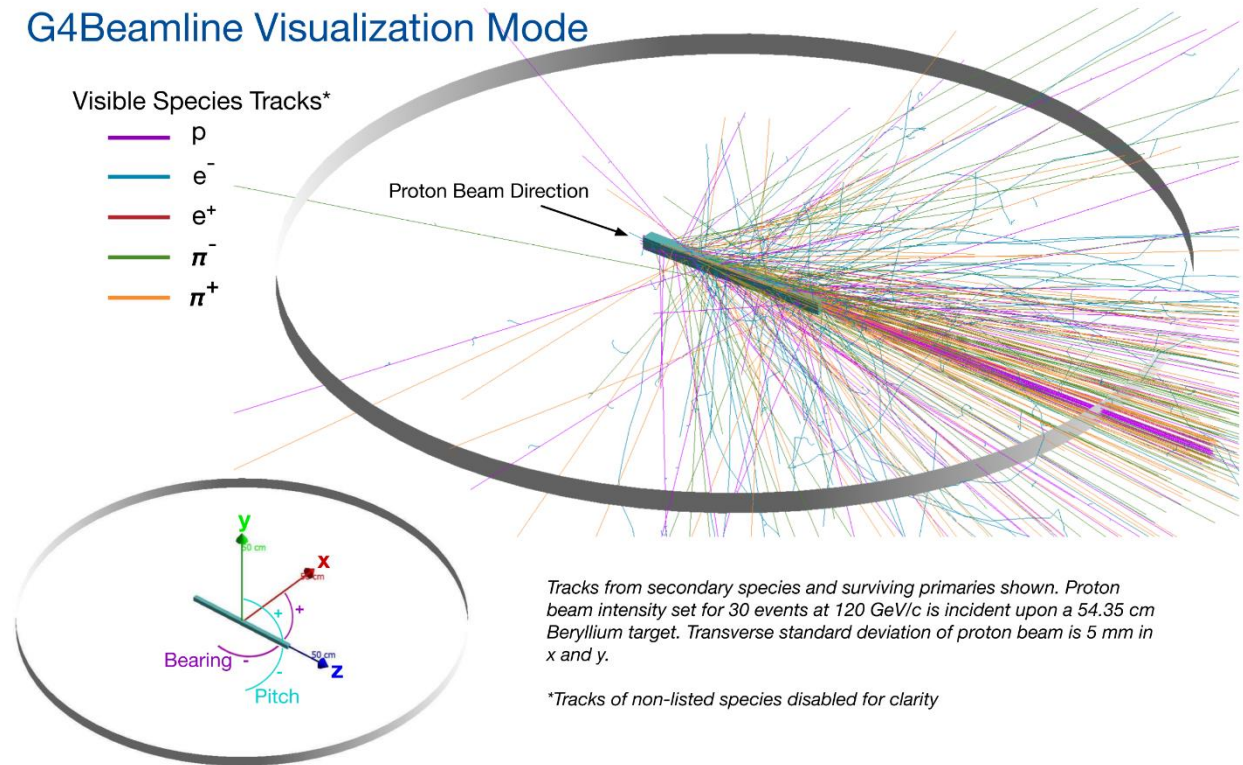


Figure 6 | Visualization of beryllium target inside ring detector after low intensity incident proton beam. Captured from G4Beamline, the redesigned virtual detector and emittance of species of interest from an incident 120 GeV/c beam with an intensity of 30 protons is shown. The cartesian coordinate system (red for positive x, green for positive y, and blue for positive z) is shown in the lower left with length scale at 50 cm for each arrow.

The detector was given a ring height of  $\pm 1$  inch in order to perform a pitch cut. An additional function of the shape was to confirm the optimal bearing angle width by allowing detection of all particles with a non-zero forward momentum ( $P_z$ ) component. It was desired to find a bearing range that contained very high energy forward-going  $\pi^\pm$  away from the central z-axis - thereby avoiding the difficulty of removing the primary and high-energy protons that populated the central forward region.

All species of particles 30 GeV/c and above were within a bearing of about  $\pm 0.4$  radians. Inspection specifically of  $\pi^\pm$  counts above 30 GeV/c showed a much narrower bearing spread of  $\pm 0.09$  radians (or  $\pm 5.16$  degrees).

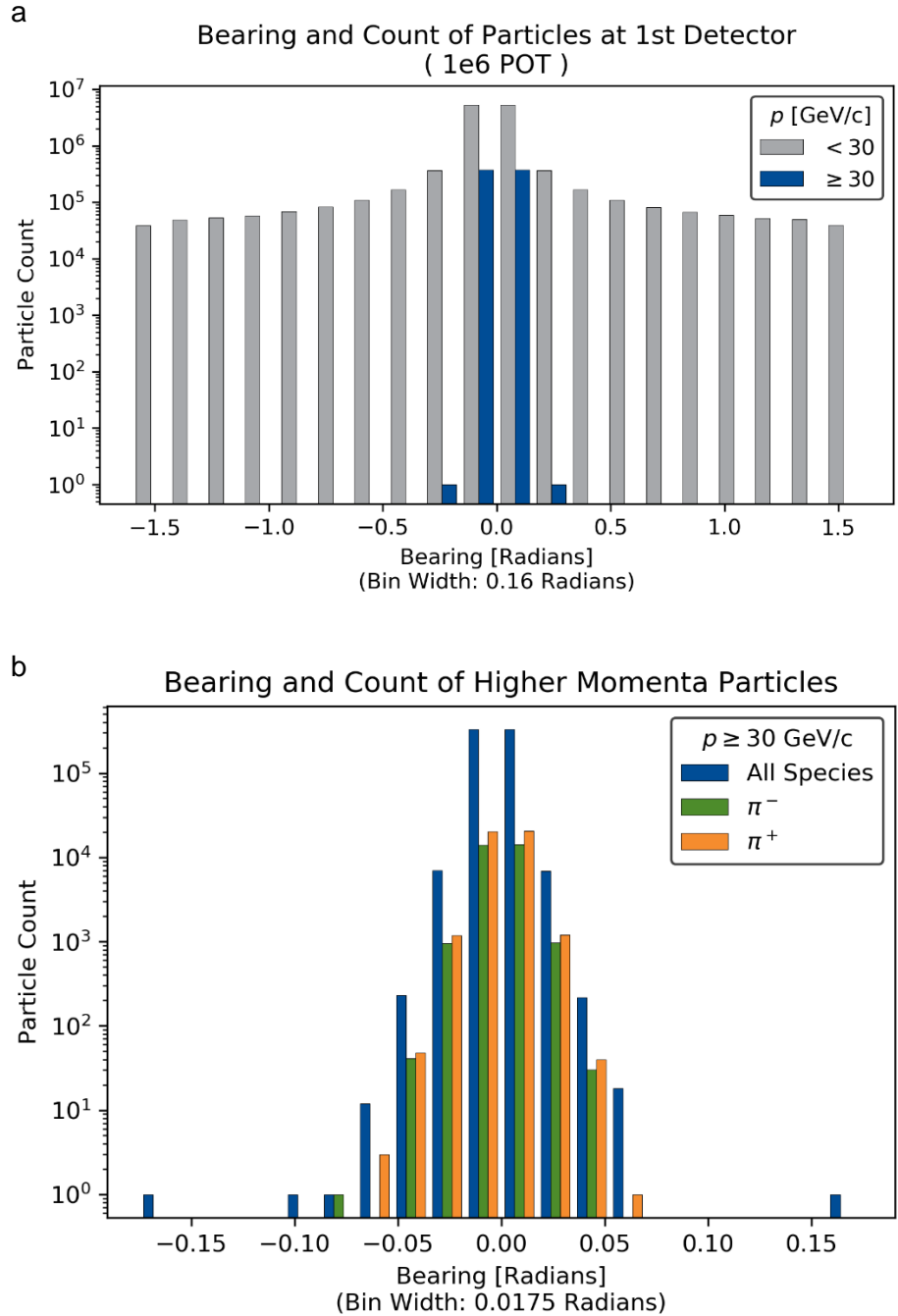


Figure 7 | Energy and Angular Distribution of All Particles and  $\pi^\pm$  Seen at Ring Detector. a. Results from  $1 \times 10^6$  protons on target show higher momentum secondary particles emitted at narrower bearing angles than the majority of lower momentum particles. b. Comparison of all particles above the momentum cut with charged pions show  $\pi^\pm$  occupying a slightly narrower angular range.

Increasingly higher energy  $\pi^\pm$  were found within smaller angular ranges, with a bearing spread for the narrow momentum range (referred to hereafter as a momentum bite) of 50 GeV/c  $\pm 5\%$  of only  $\pm 0.035$  radians.

The simulation data (which can be referred to as Monte Carlo data) confirmed the existence and location of high energy particle species of interest, as well as where the apertures of the first optical components receiving the beam would need to be placed.

Preliminary studies were also conducted to find the relationship between G4Beamline computation time and the number of events (or simulated primary particles) in a single run. Using a fixed length target, 120 GeV/c proton beam, and beginning at 10 events, several python timed simulations were run. For each consecutive run, the event number was increased by a factor of 10. Using these data points, the time per event ratio was calculated. This revealed that any event number greater than  $1 \times 10^6$  would take many hours to complete, thus an upper limit on the highest statistics that could be efficiently produced for this study was identified.

### 3.2 Triple Parameter Target Optimization

Following from the assumption that high energy  $e^\pm$  particles would come from rare pion decay, optimization of a target for maximum  $\pi^\pm$  production was performed. This would be a threefold process as the material, cross-sectional dimensions, and length would need to be independently varied.

To assist in material selection, several metrics were computed for various elements. Desiring shorter nuclear interaction lengths ( $\lambda_n$ ) and longer radiation ( $\chi$ ) and pion interaction lengths ( $\lambda_\pi$ ), the ratios of  $\lambda_n/\chi$  and  $\lambda_n/\lambda_\pi$  were computed for solid and liquid states of several elements.

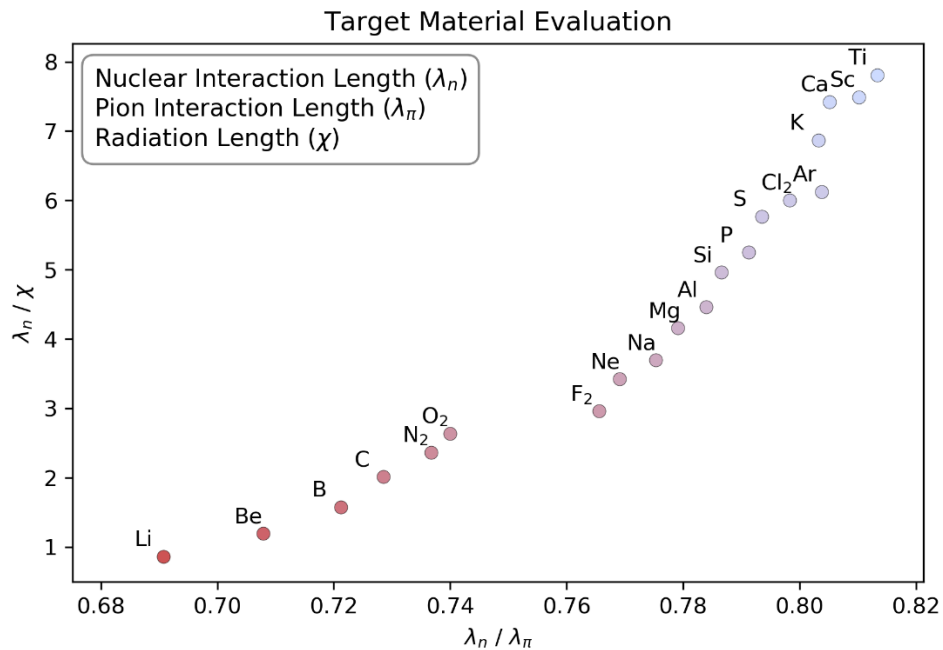


Figure 8 | Evaluation of Possible Target Materials. Materials with smaller values for both calculations were likely to yield the most  $\pi^\pm$  with minimal loss of secondary charged pions. Trends show that lighter elements possess greater production potential for charged pions.

Though lithium returned the smallest numbers, beryllium (Be) was chosen for further optimization due to in-house availability of the material.

With the selected material, the cross-sectional dimensions and length were next optimized simultaneously for  $\pi^\pm$  production. As the incident proton beam has a normal distribution of its particles in both the x and y dimensions with no angular spread, the 2-dimensional Gaussian distribution function (9) applies.

$$f(x, y) = \frac{1}{\sigma_x \sigma_y 2\pi} e^{-\frac{1}{2} \left( \frac{(x-\bar{x})^2}{\sigma_x^2} + \frac{(y-\bar{y})^2}{\sigma_y^2} \right)} \quad (9)$$

As the mean values of x ( $\bar{x}$ ) and y ( $\bar{y}$ ) are equal to zero for the given placement of the target within the coordinate system, and standard deviation in both the x dimension ( $\sigma_x$ ) and y dimension ( $\sigma_y$ ) for the proton beam was 5 mm, the amount of beam seen at different cross-sectional target dimensions was able to be calculated via integration of (9). The question of whether a thinner 20 X 20 mm<sup>2</sup> target (covering the range in x and y of  $\pm 2\sigma$  in statistical terms) that receives 91.1070% of the beam would facilitate more charged pions escaping the material, or would a thicker 30 X 30 mm<sup>2</sup> target (covering the  $\pm 3\sigma$  range in x and y) that receives 99.4608% of the beam be more effective was investigated. Production as a function of length was performed on both targets to determine which cross-sectional area and which length produced the most  $\pi^\pm$  per POT.

To approximate the length of the in-house sample, a starting length of 110 mm and a final ending length of 1,900 mm was chosen. For data points, 15 total lengths from end to end were sampled to return 15 separate Monte Carlo simulation runs. Each simulation run was then checked in Python, and the total output of  $\pi^\pm$  for a given length recorded. After normalizing to  $1 \times 10^4$  POT, these results were used to compute a fit curve. Monte Carlo returned integer counts (N) were sufficiently high enough to compute error bars using the root of N as the distance above and below the individual Monte Carlo point, and normalizing to  $1 \times 10^4$  POT.

The target length optimization returned two lengths optimal for maximal  $\pi^\pm$  production. Then, the target's dimensions were adjusted to further maximize  $\pi^-$  production and a higher intensity proton beam of  $1 \times 10^6$  was run in G4Beamline for improved statistics. The bearing or horizontal angular properties of higher momentum species of interest was then checked.

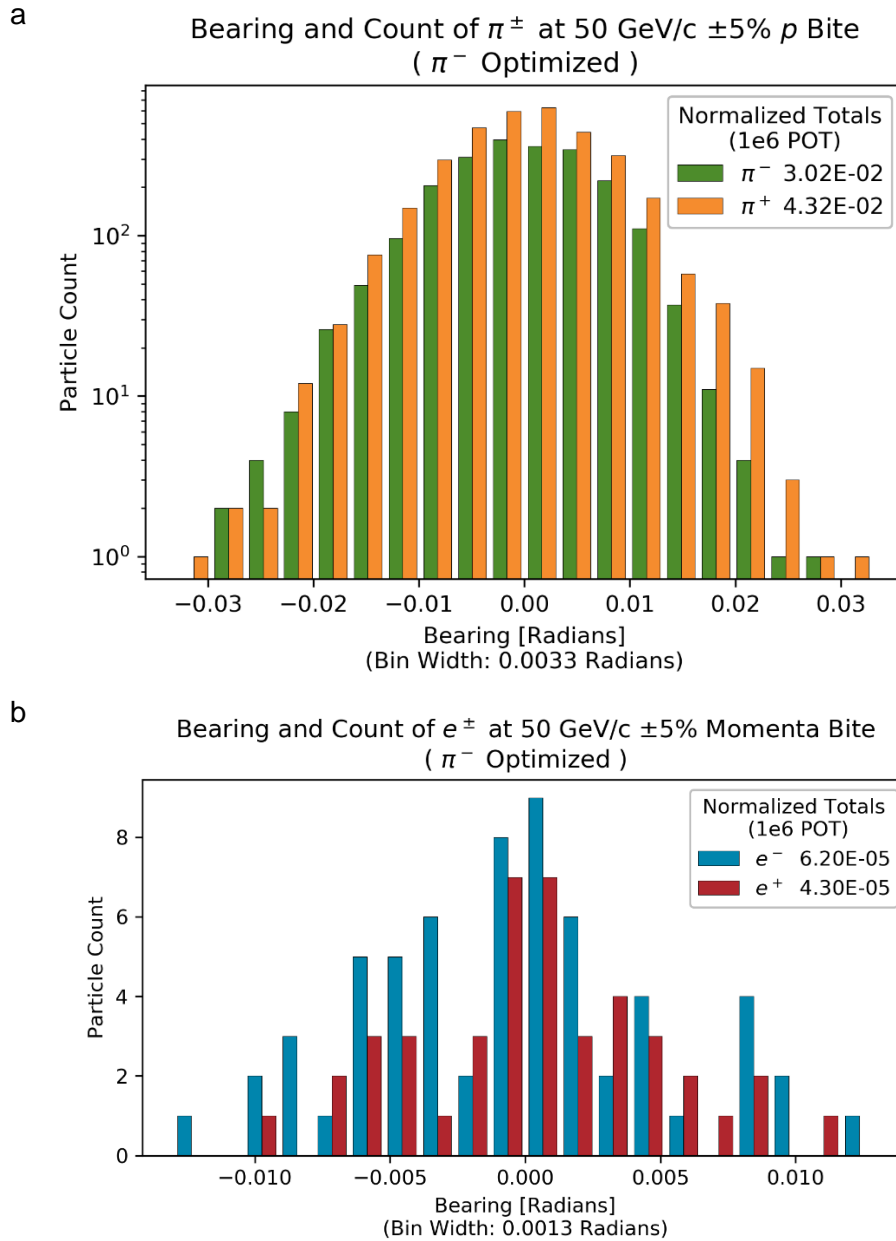


Figure 9 | Angular Distribution Comparison of Species of Interest for the 50 GeV/c Momentum Bite. a. The bearing for charged pions at a higher momentum cut is significantly narrower than the range 30 GeV/c occupies (refer to Fig. 6). b. Electrons and positrons were found to occupy a narrower bearing range than charged pions at the same momentum bite.

Using the Monte Carlo results from this run, the momentum spread and count for prompt  $e^\pm$  was checked. An unexpectedly high production of prompt  $e^\pm$  was soon found.

Momenta and Count of  $e^\pm$  at 1st Detector  
(  $\pi^-$  Optimized )

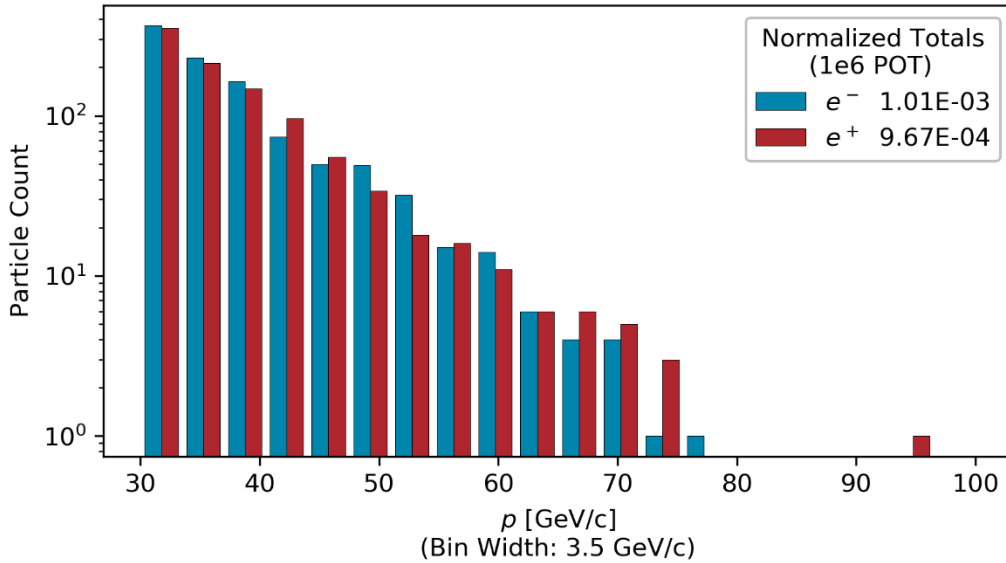


Figure 10 | Total Production and Momenta Distribution of Prompt High Energy Electrons and Positrons. Significant counts of  $e^\pm$  above the minimum energy were produced directly from the target.

To better understand the mechanism of the high energy prompt  $e^\pm$ , an investigation into the actual physics processes responsible was initiated. All processes within the FTFP\_BERT physics list (this list applies to the Fritiof FTF Model for species with energy  $>\sim 10$  GeV and the Bertini BERT Cascade Model for species  $<\sim 10$  GeV) were inspected to first identify any with the potential to create positrons or electrons. Of the 62 total processes in the list, 27 were identified for individual evaluation.

Of the 27 processes to be investigated, a single process would be disabled and all others would remain active while  $1 \times 10^6$  events (or protons of the incident beam) were run and the total count of  $e^\pm$  at or above the kinetic energy threshold would be recorded. The process would then be enabled and another process disabled before running the same number of events and recording the new data set of  $e^\pm$  counts. Once this was completed, all processes were enabled and again  $1 \times 10^6$  events was run to obtain a maximum count of  $e^\pm$  meeting the energy cut. This number was then used to normalize the  $e^\pm$  counts recorded for each run where a process was disabled, and using this generally reduced number, the normalized yield reduction could be computed as a function of the disabled process. Interestingly, several processes making up a chain reaction were found to be responsible for almost all  $e^\pm$  high energy secondaries.

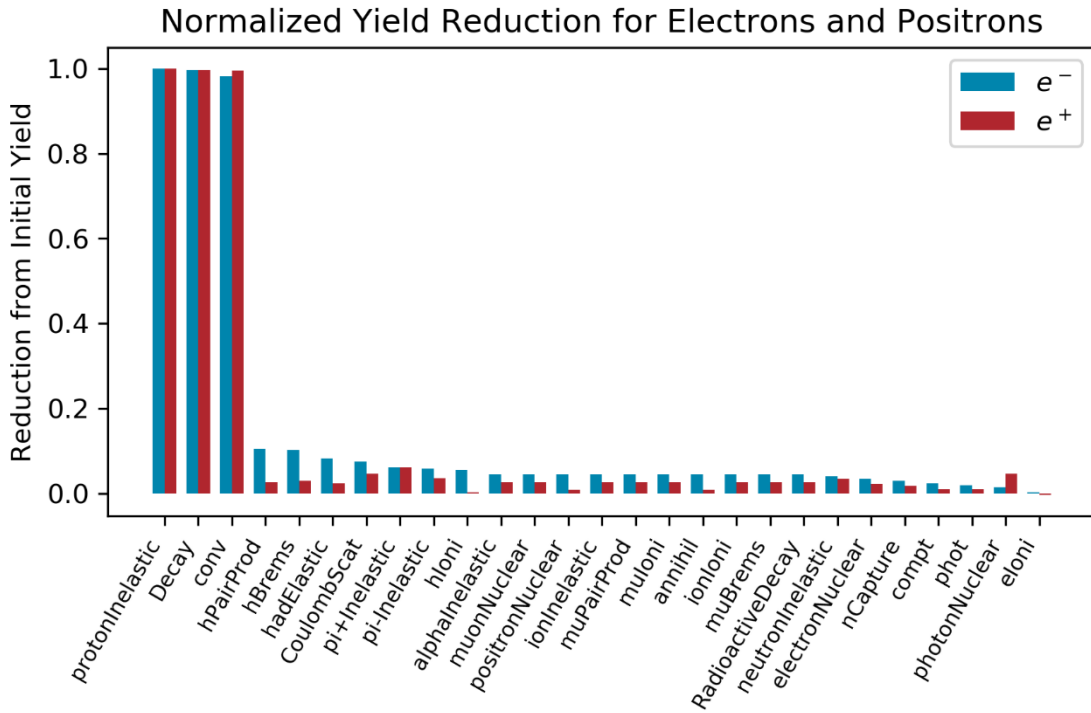


Figure 11 | Reduction to  $e^\pm$  Output for a Given Disabled Process. Disabling the proton inelastic, particle decay, or gamma conversion to  $e^+e^-$  processes severed the reaction chain responsible for nearly all prompt high energy  $e^\pm$ .

Analysis of prompt  $e^\pm$  phase space (a method of seeing how an oscillating system, such as the beam envelope, evolves through the magnetic optics by plotting particle amplitude against its position) was also conducted.

# Phase Space & Momenta Distribution

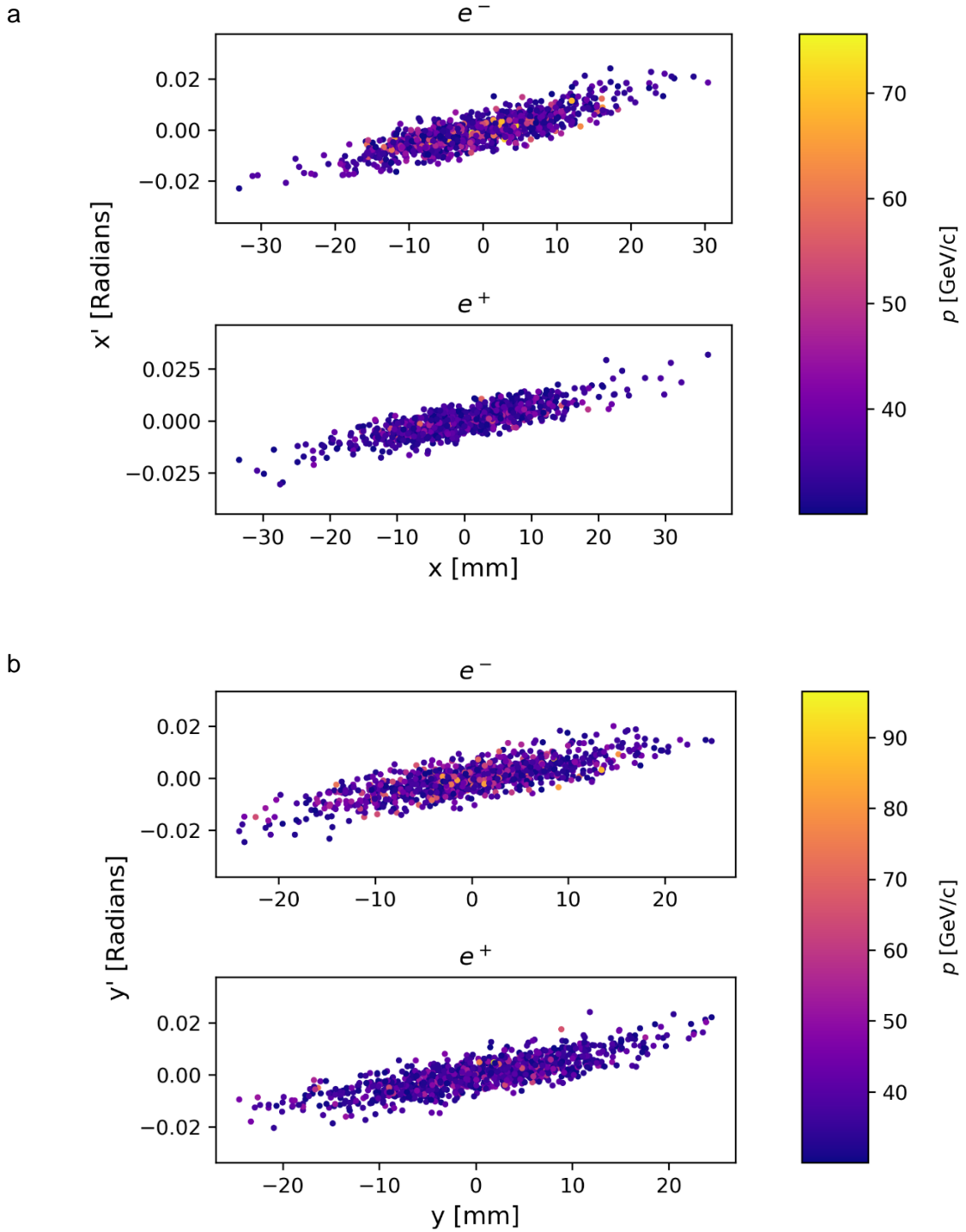


Figure 12 | Transverse Phase Space with Momenta Distribution for Prompt  $e^\pm$ . a. Referenced in the coordinate diagram of Fig. 5, the  $x$  position of  $e^\pm$  is plotted against the  $x'$  angle (the bearing). b. The  $y$  position is plotted against the  $y'$  angle (the pitch). Slightly more dispersion of higher momentum  $e^\pm$  is seen for the  $y'$  angle than that of the  $x'$  angle.



As the production for high momenta prompt  $e^\pm$  was significantly greater than expected, it was decided that new dimension optimizations for the target be conducted. Similar to the optimization for length and cross-sectional area done for  $\pi^\pm$  production,  $1 \times 10^4$  POT were used to study  $e^\pm$  prompt production. Once complete, unique optimal lengths had been identified for maximizing prompt  $e^\pm$  per POT.

Upon completion of the production optimization studies, G4Beamline was run at  $1 \times 10^6$  POT three more times using each of the three optimal lengths found for  $\pi^+$ ,  $e^+$ , and  $e^-$ . In order to identify which 2 of the 4 optimal lengths (or which two prompt species) yielded the highest intensity of  $e^\pm$  at the experiment, each of the 4 high statistics Monte Carlo files (obtained from running  $1 \times 10^6$  protons on a target optimized for a single species) would need to be analyzed.

The investigation continued using high statistics Monte Carlo data obtained from a target with dimensions set to maximize  $\pi^-$  production. Though it was planned that once the study was complete using this set of output data, it would be repeated using the Monte Carlo data obtained from optimizing the target for production of the other species and compared. Unfortunately, time limitations did not allow this.

### 3.3 Transmission and Verification of $e^\pm$ Delivery to Experiment

The next step was confirming that the minimum intensity of 5,000  $e^\pm$  per spill at the experiment location could be achieved. Ideally, this would be done after the design of optics needed to transport and species select the beam for either  $e^+$  or  $e^-$  (at different energies) was complete. In doing this, the simulation would most accurately describe what the experiment would receive. Again due to time constraints the approach taken was to select a specific energy to tune the alternating gradient focusing lattice for and design placeholder optics to collimate the beam before injecting it into the beam transport lattice. Once beam was injected into the transport channel, the momentum spread acceptance (this parameter defines the momenta that the focusing channel is able to successfully propagate without significant loss of beam) and  $e^\pm$  delivery to the test site could be studied.

To anticipate all sources of beam loss during species selection, the intensity specification at the experiment was increased to  $5 \times 10^4$   $e^\pm$ , providing a loss buffer of one order of magnitude. Additionally, the estimated distance from the target location in the M01 enclosure to the experiment location in MTest is about 500 m so this transport distance (inclusive of the total FODO lattice length) was adopted for the study.

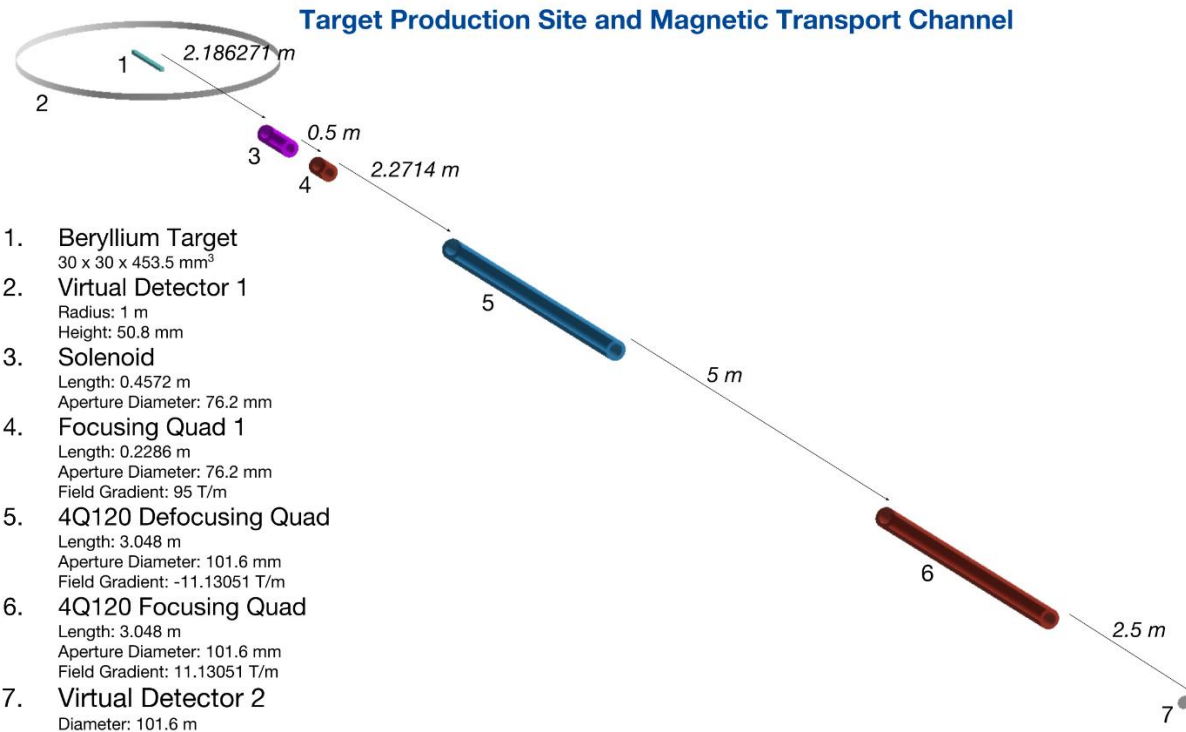


Figure 13 | Visualization of the Target, Detectors, and Optics Used for Bulk Beam Transport at 50 GeV/c Momentum Bite. The defocusing quad 5 followed by drift space and focusing quad 6 make up the basic FODO cell used in the bulk transport study.

Capture of the secondary production beam was done using a 0.4572 m solenoid with an aperture diameter of 3". The upstream end was placed 2.186271 m downstream from the center of the target, with z-axis oriented on its central axis. The exit of the solenoid was then separated from a 0.2286 m long focusing quad by 0.5 m. The gradient of this quadrupole was set to 95 T/m and it was also given a 3" aperture to perform emittance matching to the FODO lattice. The solenoid served as a first-pass placeholder solution for the capture optics (this will be replaced with a technically realizable system on the next optics iteration, possibly a lithium lens). Placed 2.2714 m from the exit of the first quad is a defocusing quad with 4" aperture and 120" in length (referred to as a 4Q120) which is the first component in the FODO cell transport lattice. Separated by 5 m from a focusing 4Q120, these magnets form a FODO cell. Alternating gradients of -11.13051 T/m in the defocusing and 11.13051 T/m in the focusing 4Q120s were used. The presence and strength of these fields was verified in G4Beamline by creating 3 virtual detectors for each device. One detector was placed inside the device near the upstream side, another at the center, and the last closer to the downstream end. Monte Carlo settings were adjusted to include magnetic field information experienced by the particles, and  $1 \times 10^4$  primary proton events were run to confirm desired field strengths.

After placing a 4" diameter virtual detector 2.5 m downstream from the focusing 4Q120, the data file from the Monte Carlo run for  $1 \times 10^6$  events on a  $\pi^-$  optimized target was used for the beam input for the downstream optics. This particle data file was then propagated down the line and results at the detector were written to a new file and analyzed. The defocusing and focusing 4Q120 cell structure was then repeated with the same separation distance of 5 m between each

quad maintained and the detector placed 2.5 m past the last quad. The last Monte Carlo file written was then used for the transported beam information and then propagated down the line to the next detector location. This pattern was repeated for the first 6 repetitions of the lattice to study the lattice acceptance from upstream at the first FODO cell over the first 100 m of flight.

The beam composition for  $e^\pm$  and  $\pi^\pm$  was then examined at every successive 100 m until reaching the experiment at 500 m. The momentum bite transported by the acceptance of the FODO cell lattice was also studied. Once at the experiment, final results for total numbers of  $e^\pm$  delivered were recorded.

## 4. Results

### 4.1 Optimizing for $\pi^\pm$ Production

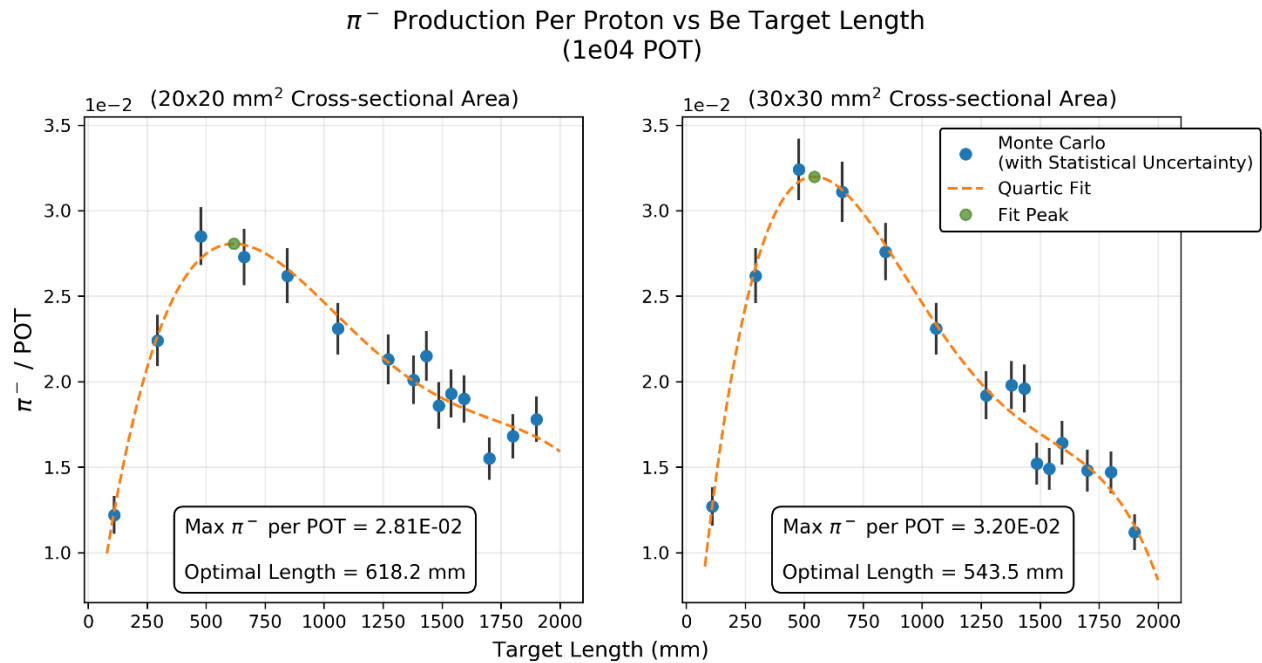


Figure 14 | Dimensional Optimization for Maximizing  $\pi^-$  Production. The peak from the fit line indicates that a maximal  $\pi^-$  per POT of  $3.20 \times 10^{-2}$  is produced when a  $30 \times 30 \times 543.5 \text{ mm}^3$  target is used. Error bars show that Monte Carlo spanning the fitted peak are within  $1\sigma$  of one another, giving confidence in the analysis.

$\pi^+$  Production Per Proton vs Be Target Length  
(1e04 POT)

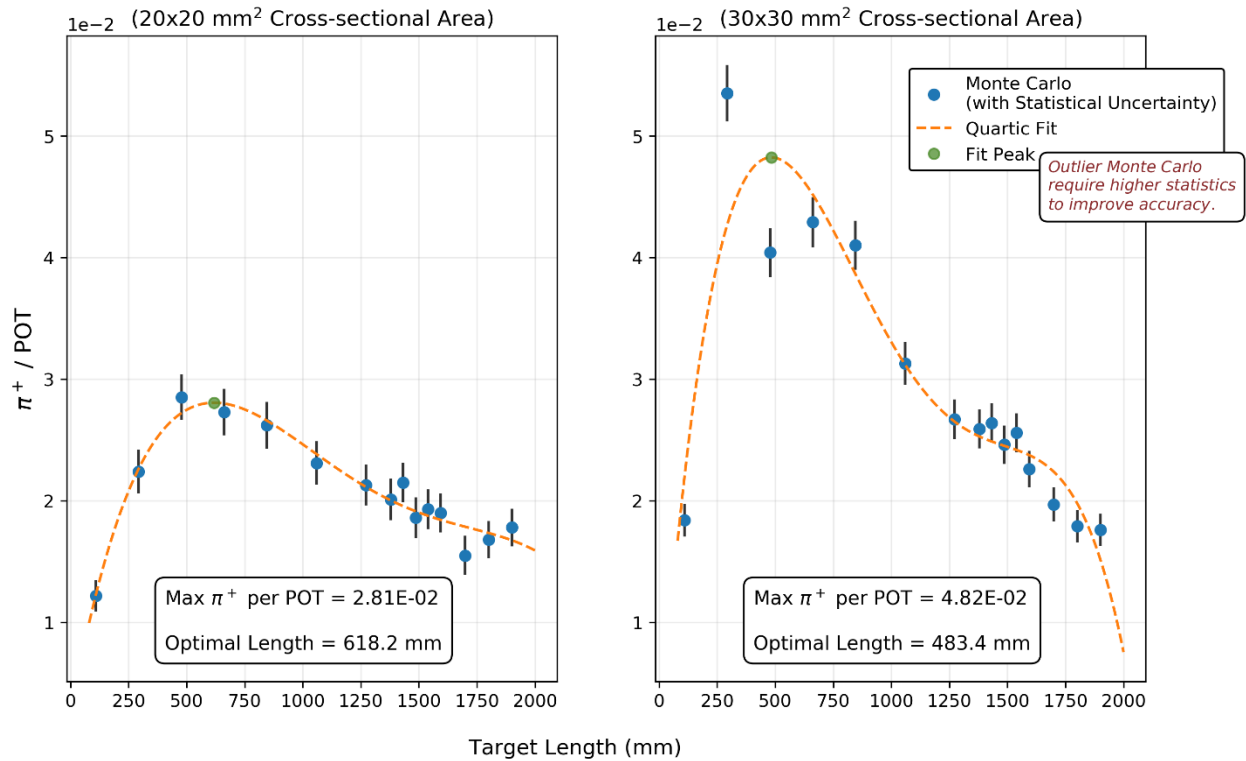


Figure 15 | Dimensional Optimization for Maximizing  $\pi^+$  Production. The fitted peak showing a maximum  $\pi^+$  per POT of  $4.82 \times 10^{-2}$  occurs for a  $30 \times 30 \times 483.4 \text{ mm}^3$  target. Error bars however indicate that Monte Carlo data are outside the fitted peak and beyond  $1\sigma$ . Spacing indicates that more simulation trials at smaller intervals across the peak might be necessary to confirm the accuracy of the fit.

## 4.2 Optimizing for Prompt $e^\pm$

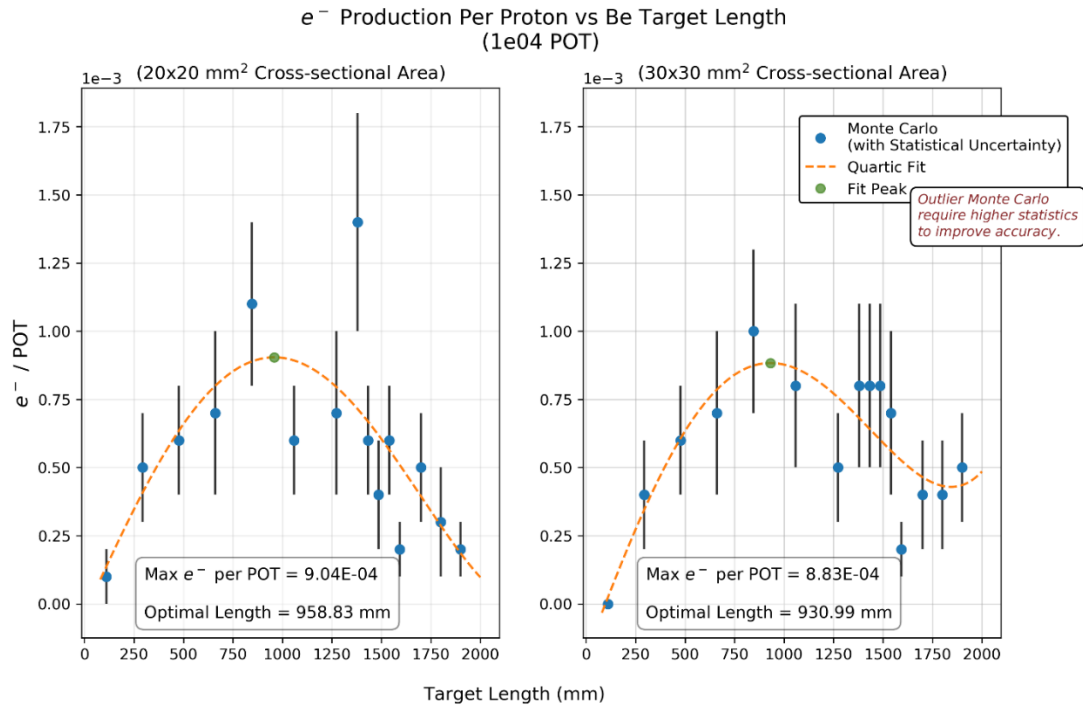


Figure 16 | Dimensional Optimization for Prompt Electron Production. The fitted peak shows that the maximum  $e^-$  per POT of  $9.04 \times 10^{-4}$  occurs when a 20 X 20 X 958.83 mm<sup>3</sup> target is used. Though Monte Carlo globally appears to be within  $1\sigma$  of neighboring points, the presence of an outliers may be skewing the fit. Higher statistics are needed to confirm as trends in optimal cross-sectional area favor 30 X 30 mm<sup>2</sup>.

### $e^+$ Production Per Proton vs Be Target Length (1e04 POT)

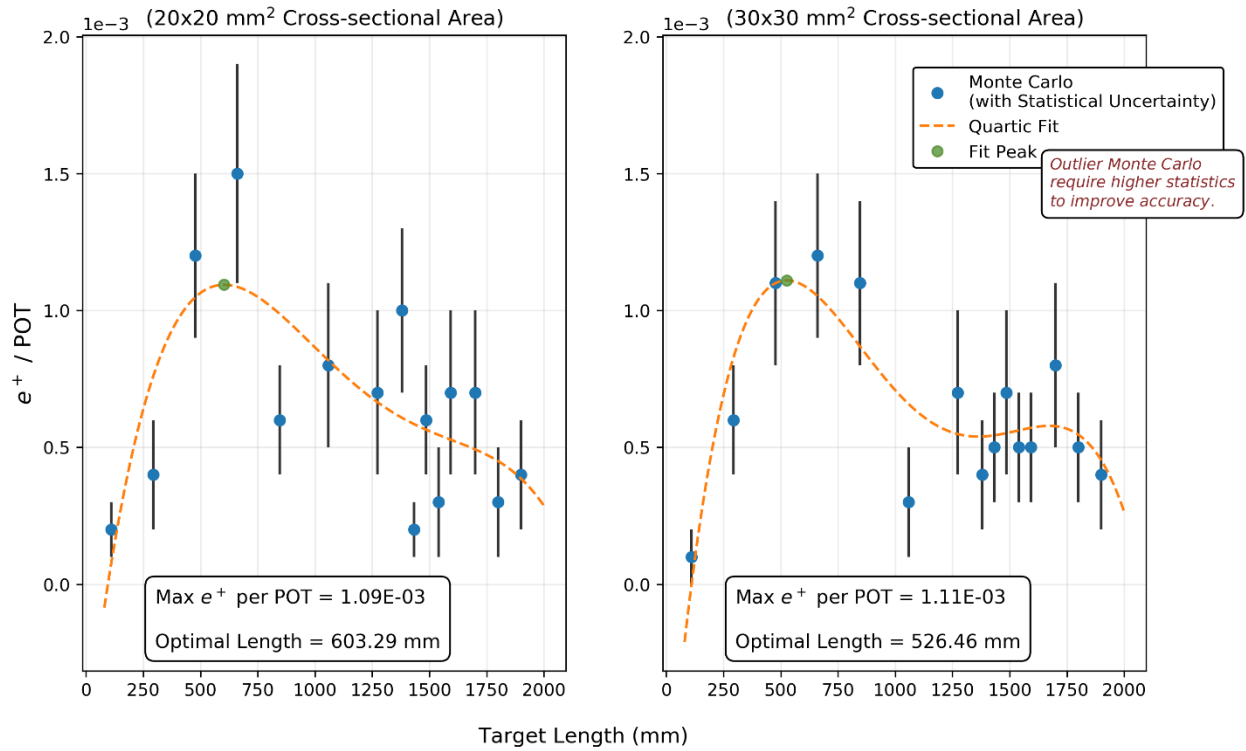


Figure 17 | Dimensional Optimization for Prompt Positron Production. The fitted peak indicated a maximal  $e^+$  per POT of  $1.11 \times 10^{-3}$  for a  $30 \times 30 \times 526.46 \text{ mm}^3$  target. The fit falls within  $1\sigma$  of the Monte Carlo data points.

### 4.3 Lattice Acceptance

Intensity of Momenta Distribution with Magnetic Transport

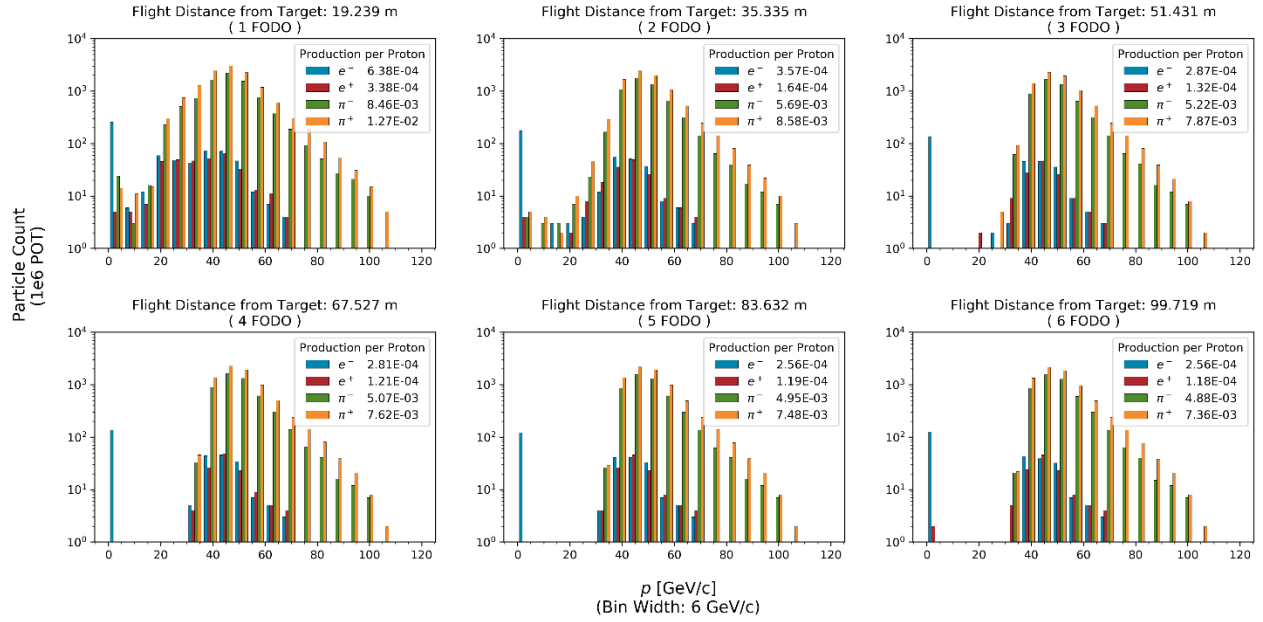


Figure 18 | Propagation of Beam Down the FODO Lattice for First 100 m of Flight. Normalized counts calculated after each of the first 6 successive FODO cells show initial loss of most particles below 30 GeV/c.

Intensity of Momenta Distribution with Magnetic Transport

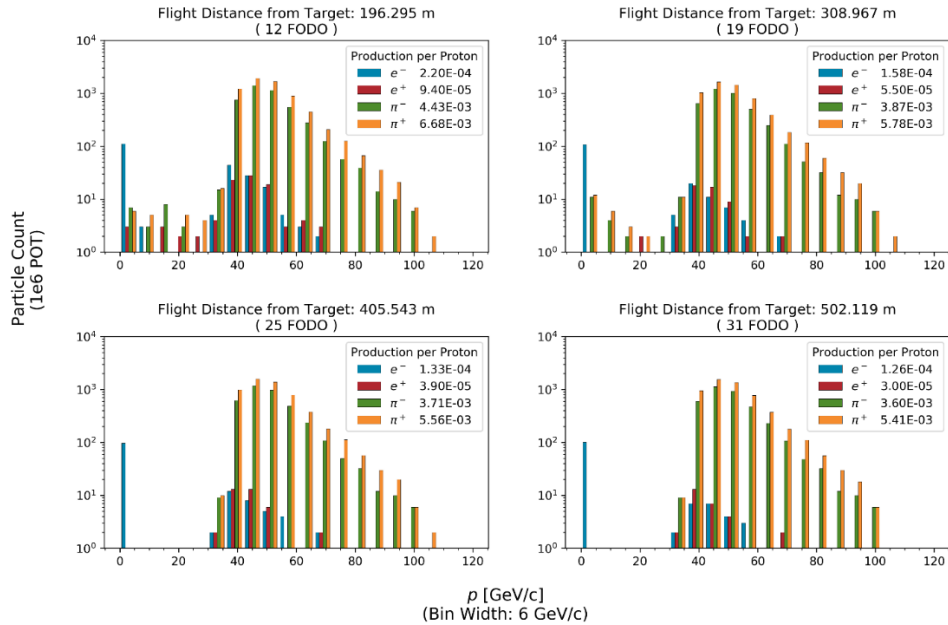


Figure 19 | Momenta Range Detected Every 100 m for  $e^\pm$  and  $\pi^\pm$ . Though lower momenta particles are present at the 200 and 300 m distances, they do not survive. Particles within the 30 to 60 GeV/c range reached the experiment despite steady decrease in their numbers.

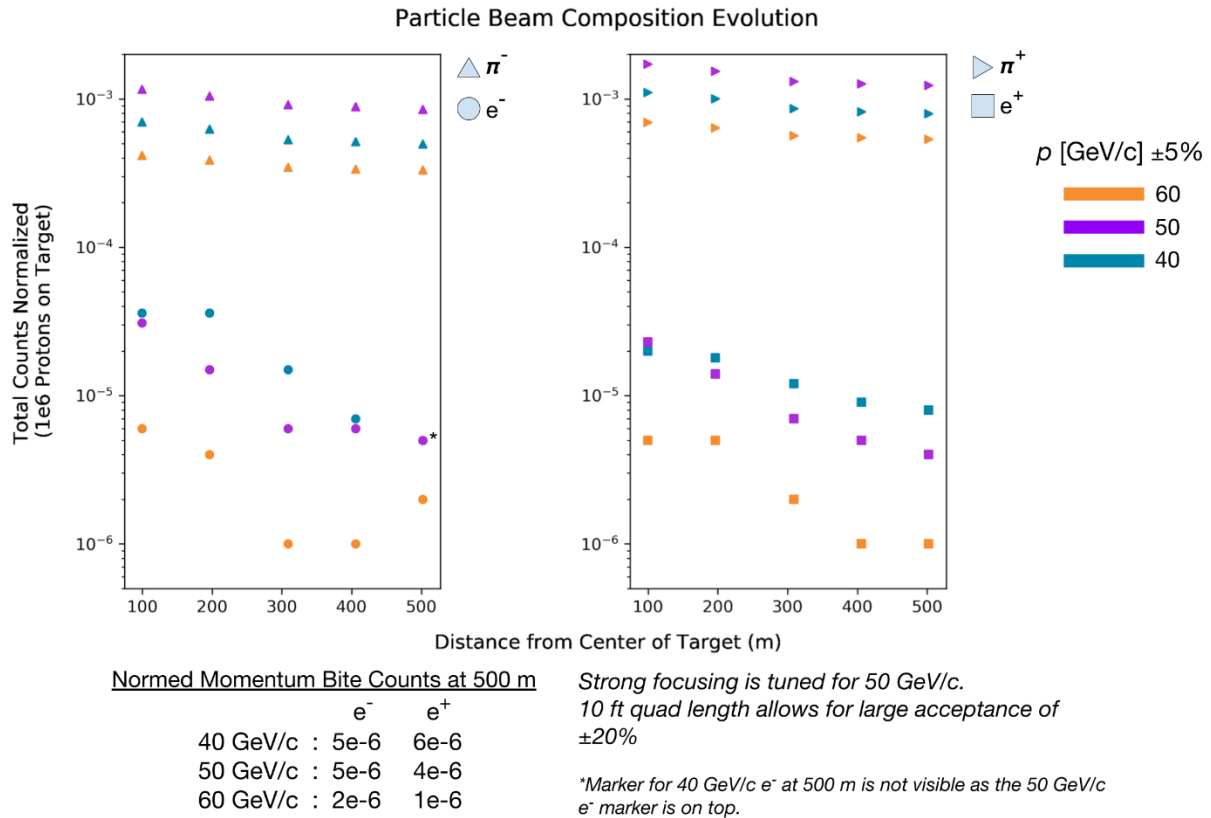


Figure 20 | Change in Production of e<sup>±</sup> and π<sup>±</sup> Leading to the Experiment for the 40, 50, and 60 GeV/c Momentum Bites. The steepness of earlier drops in e<sup>±</sup> production over the first couple hundred meters likely indicates that the lattice may be slightly mismatched to the beam or that the apertures are shaping the captured beam into a matched phase space ellipse (an elliptical phase space is the dynamically stable shape cross-section for the beam).

Though all species undergo beam loss during transport, π<sup>±</sup> experience a much lower rate of loss. Losses from the expected decay in flight are likely the primary contributors.

The successful transmission of 40, 50, and 60 GeV electrons and positrons implies that the lattice is in fact tuned for 50 GeV/c but has a very large acceptance of about ±20%.



#### 4.4 Delivered $e^\pm$ Beam Intensity

Expected Momentum Bite Intensity with 1 Order of Loss				
$p$ Bite [GeV/c] $\pm 5\%$	MT4 Proton Intensity: $2e11$		MT1 Proton Intensity: $1e13$	
	$e^-$	$e^+$	$e^-$	$e^+$
40	$1e5$	$1.2e5$	$5e6$	$6e6$
50	$1e5$	$8e4$	$5e6$	$4e6$
60	$4e4$	$2e4$	$2e6$	$1e6$

Table 3 | Intensity of Electrons and Positrons Delivered to the Experiment for Current Proton Beam Intensities. The minimal  $e^\pm$  intensity needed at the 500 m experiment site has been exceeded for all 3 energies (nearly identical to the momenta magnitudes) studied.

Assuming the target would be set up at the current MT4 target station and estimating maximum loss during species selection to be an additional order of magnitude of the total transported in this simulation, a  $2 \times 10^{11}$  primary proton beam would yield  $e^-$  beam intensities of  $1 \times 10^5$  for both 40 and 50 GeV bites, and  $4 \times 10^4$  for the 60 GeV bite.

For  $e^+$  beam intensities after losses,  $1.2 \times 10^5$  is predicted for 40 GeV,  $8 \times 10^4$  for 50 GeV, and  $2 \times 10^4$  for the 60 GeV bite.

For even higher secondary intensities, set up of the production target at the higher intensity MT1 target station would allow the highest intensity proton beam at  $1 \times 10^{13}$  protons. Assuming order of magnitude losses,  $e^-$  beam intensities of  $5 \times 10^6$  for 40 and 50 GeV, and  $2 \times 10^6$  for the 60 GeV bite were achieved in simulation. With the same loss assumptions,  $e^+$  beam intensities of  $6 \times 10^6$  for 40 GeV,  $4 \times 10^6$  for 50 GeV, and  $1 \times 10^6$  for the 60 GeV bite are correspondingly achieved.

### 5. Conclusion

This feasibility study has shown that it is possible to create a high energy, high purity  $e^\pm$  test beam from secondary particle production from a target at Fermilab. It is clear that the current 120 GeV proton beam intensities available are more than adequate to meet these goals when used on a Be production target.






Continued study should result in a better optimization and improved rates. As the target length used for  $\pi^-$  production differs significantly from the optimal length for maximum prompt  $e^-$  from a  $30 \times 30 \text{ mm}^2$  target, adjusting this length should increase the prompt  $e^-$  production by 22.8 %. Such metrics indicate that there remains much to consider in designing the optimal  $e^\pm$  beam, particularly, as the physics source of high energy prompt electrons and positrons has yet to be isolated. Once identified, new optimization parameters can be developed which may yield even higher secondary energies and intensities for future user experimental facilities.

## References

1. "H2 Beam Line." Cern.ch, CERN, 2017, <http://sba.web.cern.ch/sba/BeamsAndAreas/resultbeam.asp?beamline=H2>. Accessed 29 July 2018.
2. "Test Beams at DESY." Desy.de, Deutsches Elektronen-Synchrotron DESY, 2013, [particle-physics.desy.de/e252106/](http://particle-physics.desy.de/e252106/). Accessed 29 July 2018.
3. "FACET-II Overview." Stanford.edu, Stanford University, 2016, <https://facet.slac.stanford.edu/overview>. Accessed 29 July 2018.
4. Pocanic, Dinko et al. "Experimental study of rare charged pion decays." Journal of Physics G: Nuclear and Particle Physics. Volume 41 Issue 11. 2014: 34 pg. iop.org. Web. <http://iopscience.iop.org/article/10.1088/0954-3899/41/11/114002>. Accessed 29 July 2018
5. Halkiadakis, Eva. "Lecture 3: Particle Interactions with Matter." Rutgers.edu, Rutgers University, 2009. [www.physics.rutgers.edu/~evahal/talks/tasi09/TASI\\_day3\\_school.pdf](http://www.physics.rutgers.edu/~evahal/talks/tasi09/TASI_day3_school.pdf) Accessed 29 July 2018. Accessed 30 July 2018.
6. Watts, Adam, et al. "Concepts Rookie Book." Fermilab Accelerator Division. PDF. December 3, 2013.
7. "G4beamline Release 3.04 Is Available (March 2017)." Muonsinternal.com, Muons Inc., [www.muonsinternal.com/muons3/G4beamline#Documentation](http://www.muonsinternal.com/muons3/G4beamline#Documentation). Accessed 30 July 2018.
8. "Geant4 Scope of Application." Cern.ch, GEANT4 Collaboration, <http://geant4-userdoc.web.cern.ch/geant4-userdoc/UsersGuides/IntroductionToGeant4/html/IntroductionToG4.html>. Accessed 30 July 2018.
9. "Monte Carlo Method." Encyclopædia Britannica, Encyclopædia Britannica, Inc., 26 Sept. 2017, [www.britannica.com/science/Monte-Carlo-method](http://www.britannica.com/science/Monte-Carlo-method). Accessed 29 July 2018. Accessed 30 July 2018.
10. "Longer Term LHC Schedule." Cern.ch, CERN, <https://lhc-commissioning.web.cern.ch/lhc-commissioning/schedule/LHC-long-term.htm>. Accessed 15 August 2018.

## Acknowledgements

A special thanks to those whose patience and willingness to share their knowledge made this work possible:

-  Carol Johnstone
-  Adam Watts
-  Jason St. John
-  John Johnstone
-  Tom Roberts

This manuscript has been authored by Fermi Research Alliance, LLC under Contract No. DE-AC02-07CH11359 with the U.S. Department of Energy, Office of Science, Office of High Energy Physics.